Responses of Arctic Black Carbon and Surface Temperature to Multi-Region Emission Reductions: an HTAP2 ensemble modeling study

Na Zhao[1], Xinyi Dong[2], Kan Huang[1]*, Joshua S. Fu[3,4*], Marianne Tronstad Lund[5], Kengo Sudo[6], Daven Henze[7], Tom Kucsera[8], Yun Fat Lam[9], Mian Chin[10], Simone Tilmes[11]

[1] Shanghai Key Laboratory of Atmospheric Particle Pollution and Prevention (LAP3), Department of Environmental Science and Engineering, Fudan University, Shanghai, China
[2] School of Atmospheric Science, Nanjing University, Nanjing, China
[3] Department of Civil and Environmental Engineering, The University of Tennessee, Knoxville, Tennessee, USA.
[4] Computational Earth Science Group, Computational Sciences and Engineering Division, Oak Ridge National Laboratory, Oak Ridge, Tennessee, USA.
[5] CICERO Center for International Climate and Environmental Research, Oslo, Norway
[6] Nagoya University, Furo-cho, Chigusa-ku, Nagoya, Japan
[7] Department of Mechanical Engineering, University of Colorado, Boulder, CO, USA
[8] Universities Space Research Association, Greenbelt, MD, USA
[9] Department of Geography, The University of Hong Kong, HKSAR, China
[10] Earth Sciences Division, NASA Goddard Space Flight Center, Greenbelt, MD, USA
[11] Atmospheric Chemistry Observations and Modeling Laboratory, National Center for Atmospheric Research, Boulder, Colorado, USA

Correspondence: huangkan@fudan.edu.cn; jsfu@utk.edu

ABSTRACT

Black carbon (BC) emissions play an important role in regional climate change of the Arctic. It is necessary to pay attention to the impact of long-range transport from regions outside the Arctic as BC emissions from local sources in the Arctic were relatively small. The Task Force Hemispheric Transport of Air Pollution Phase2 (HTAP2) set up a series of simulation scenarios to investigate the response of BC in a given region to different source regions. This study investigated the responses of Arctic BC concentrations and surface temperature to 20% anthropogenic emission reductions from six regions in 2010 within the framework of HTAP2 based on ensemble modeling results. Emission reductions from East Asia (EAS) had most (monthly contributions: 0.2 - 1.5 ng m^{-3}) significant impact on the Arctic near surface BC concentrations while the monthly contributions from Europe

(EUR), Middle East (MDE), North America (NAM), Russia-Belarus-Ukraine (RBU), and South Asia (SAS) were 0.2–1.0 ng m^{-3}, 0.001–0.01 ng m^{-3}, 0.1–0.3 ng m^{-3}, 0.1–0.7 ng m^{-3}, 0.0–0.2 ng m^{-3}, respectively. The responses of the vertical profiles of the Arctic BC to the six regions were found to be different due to multiple transport pathways. Emission reductions from NAM, RBU, EUR, and EAS mainly influenced the BC concentrations in low troposphere of the Arctic, while most of the BC in the upper troposphere of the Arctic derived from SAS. The response of the Arctic BC to emission reductions of six source regions became less significant with the increase of the latitude. The benefit of BC emission reductions in terms of slowing down surface warming in the Arctic was evaluated by using Absolute Regional Temperature-change Potential (ARTP). Compared to the response of global temperature to BC emission reductions, the response of Arctic temperature was substantially more sensitive, highlighting the need for curbing global BC emissions.

1. Introduction

Black carbon (BC) is one of the short-lived climate forcers (SLCFs, AMAP, 2015) and was regarded as the second largest contributor to global warming, only inferior to carbon dioxide (Bond et al. 2013). BC over the Arctic can perturb the radiation balance in a number of ways. Direct aerosol forcing occurred through absorption or scattering of solar (shortwave) radiation. BC is the most efficient atmospheric particulate species at absorbing visible light (Bond et al., 2013), the added atmospheric heating will subsequently increase the downward longwave radiation to the surface and warm the surface (AMAP, 2011). Radiative forcing by BC can also result from aerosol-cloud interactions that affected cloud microphysical properties, albedo, extent, lifetime, and longwave emissivity (Twomey 1977; Garrett and Zhao 2006). BC has an additional forcing mechanism after depositing onto snow and ice surfaces (Clarke and Noone, 1985). The surface albedo of snow and ice could be reduced and further enhanced the absorption of solar radiation at the surface. In the Arctic, surface temperature responses were strongly linked to surface radiative forcing as the stable atmosphere of the region prevented rapid heat exchange with the upper troposphere (Hansen and Nazarenko, 2004).

The Arctic has been warming twice as rapidly as the world in the past fifty years, and has experienced significant changes in its ice and snow covers as well as permafrost (AMAP, 2017).

Reductions of carbon dioxide emissions are the backbone of any meaningful effort to mitigate climate forcing. But even if significant reductions of carbon dioxide are made, slow down of the temperature rise in the Arctic and the sea level rise caused by the melting of glaciers may not be achieved in time. Hence, the goal of slowing down the deterioration of the Arctic may best be achieved by also targeting at shorter-lived climate forcing agents, especially those that could impose appreciable surface forcing and trigger regional-scale climate feedbacks pertaining to the melting of sea ice and snow. Modelling studies by UNEP/WMO (2011) and Stohl et al. (2015) suggested that the climate response of SLCFs mitigation was strongest in the Arctic region. AMAP (2011 and 2015) as well as Sand et al. (2016) demonstrated that per unit of emission reductions of SLCFs in the Northern areas had the largest temperature response on the Arctic, with the Nordic countries (Denmark, Finland, Iceland, Norway, and Sweden) and Russia having the largest impact compared to other Arctic countries such as the United States and Canada.

The few studies that investigated specific regional aerosol forcing (Shindell and Faluvegi, 2009; Shindell et al., 2012; Teng et al., 2012) typically used a single climate model at a time to investigate the climate response to idealized, historical, or projected forcing. However, different models varied considerably in the representation of aerosols and radiative properties, resulting in large uncertainties in simulating the aerosol radiative forcing (Myhre et al., 2013b; Shindell et al., 2013). When investigating the climate response to regional emissions, such uncertainties were likely to be confounded even further by the variability between models in regional climate and circulation patterns and variation in the global and regional climate sensitivity (the amount of simulated warming per unit radiative forcing). Hence, the Task Force Hemispheric Transport of Air pollution Phase2 (HTAP2, http://www.htap.org/) incorporating multiple global models can avoid the great uncertainty of single model to a certain degree, with the aim to improve model estimates of the impacts of intercontinental transport of air pollutants on climate, ecosystems, and human health (Galmarini et al., 2017). To date, the HTAP2 results have been explored from a variety of scientific and policy-relevant perspectives. For instance, by comparing against observations, sulfur and nitrogen depositions during HTAP2 had been significantly improved compared to HTAP1. From 2001 to 2010, the global nitrogen deposition increased 7% while the global sulfur deposition decreased 3% (Tan et al., 2018a). The significant impacts of hemispheric transport on the deposition were specifically focused and the deposition over the coastal regions was more sensitive to

hemispheric transport than the non-coastal continental regions (Tan et al., 2018b). Jonson et al. (2018) assessed the contributions from different world regions to European ozone levels and contributions from the non-European regions were mostly from North. America and eastern Asia, larger than those from European emissions. Hogrefe et al. (2018) found that the simulated ozone over the continental US varied very differently by digesting boundary conditions from four hemispheric or global models. The impact of emission changes from six major source regions on global aerosol direct radiative forcing was estimated (Stjern et al., 2016). In the local source regions, the radiative forcing associated with SO_4^{2-} was strengthened (25%) while that from BC was weakened (37%) due to a 20% emission reduction. Liang et al. (2018) estimated global air-pollution-related premature mortality from exposure to $PM_{2.5}$ and ozone and the interregional transport lead to more deaths through changes in $PM_{2.5}$ than in O_3. However, the source region contributions to Arctic BC and the spread among multi-model results have been rarely explored from the perspective of HTAP2 initiative.

This study aims to investigate the responses of Arctic BC concentrations and surface temperature to 20% anthropogenic emission reductions from different regions in the Northern Hemisphere (NH). A comparison of six global modeling works within the framework of HTAP2 experiments for the Arctic region in 2010 was presented. The ensemble modeling results were used to apportion the contribution from different source regions to the near-surface and vertical black carbon in the Arctic. In addition, the Arctic surface temperature responses to the emission reductions were estimated.

2. Methodology

2.1 HTAP2 experiments

HTAP2 developed a harmonized emissions database covering all countries and the major sectors for global and regional modeling from 2008 to 2010. The emissions database was obtained from the nationally reported emissions (e.g., National Emission Inventory for the United States), the regional scientific inventories (e.g., European Monitoring and Evaluation Programme (EMEP), Netherlands Organisation for Applied Scientific Research (TNO) for Europe, Model Inter-Comparison Study for Asia, MICS–Asia III), and the Emissions Database for Global Atmospheric Research data (EDGARv4.3, emissions for South America, Africa, Russia and Oceania). Biomass burning

emissions were not prescribed in HTAP2. It was recommended that modeling groups used the Global Fire Emissions Database (GFED4, http://globalfiredata.org/) with a temporal resolution of daily or 3–hour intervals. The detailed information of different regional inventories can be found in Janssens–Maenhout et al. (2015).

Emission perturbations were conducted in sensitivity simulations to investigate the response of various air pollutants in a given region to different source regions. In this study, the Arctic region was the targeted receptor region of interest. Six source regions in HTAP2 experiments, namely, East Asia (EAS), Europe (EUR), Middle East (MDE), North America (NAM), Russia–Belarus–Ukraine (RBU), and South Asia (SAS) were selected to demonstrate their influences on the BC concentrations over the Arctic region (Figure 1a). Two emission scenarios were designed for the HTAP2 simulation to explore the source/receptor relationships, i.e. the base scenario (BASE) with no emission reduction, and the control scenario (EASALL, EURALL, MDEALL, NAMALL, RBUALL, and SASALL) with 20% reduction of all anthropogenic emissions in six regions respectively.

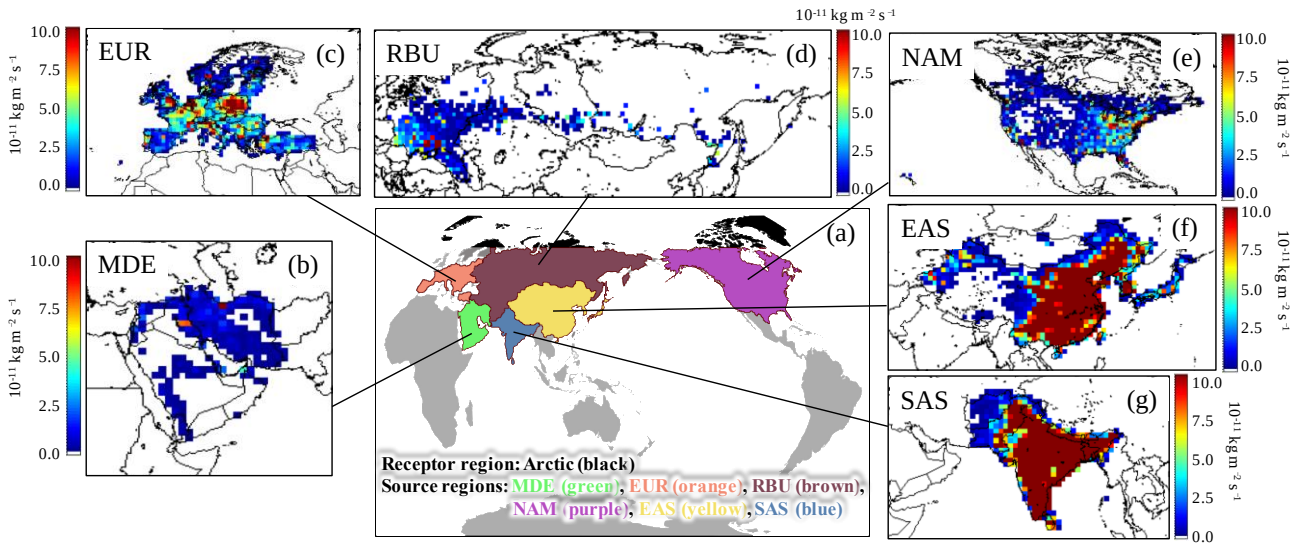

Figure 1. (a) The sketch map of receptor and source regions. **(b)–(g)** Spatial distributions of 20% reduction of annual BC emission in the six source regions in 2010. MDE: Middle East; EUR: Europe; RBU: Russia–Belarus–Ukraine; NAM: North America; EAS: East Asia; SAS: South Asia. The unit legends from (b) to (g) are the same of 10^{-11} kg m^{-2} s^{-1}.

2.1.1 Anthropogenic emission reductions of BC in HTAP2

Anthropogenic BC emission sectors included power plants, industries, transportation, shipping, aviation, agriculture, and residential sectors. The emission inventory had a monthly temporal

resolution and a spatial resolution of 0.1° × 0.1°. The total anthropogenic emissions and 20% emission reductions of BC in six source regions of HTAP2 in 2010 are presented in Table 1. The higher BC emission reductions were found in the EAS and SAS with the values of 355.6 and 232.5 Gg yr^{-1}, respectively, while were much lower in the MDE and RBU with the values of 5.3 and 18.6 Gg yr^{-1}, respectively. The BC emission reductions in the EAS, EUR, and RBU showed significant monthly variations with higher values from November to March, while the monthly variations were not obvious in the MDE, NAM, and SAS.

Table 1. 20% emission reductions and total anthropogenic emissions of BC in different regions of HTAP2 in 2010. (Unit: Gg yr^{-1}).

Regions	Total anthropogenic emissions	20% Emission Reductions												
		Jan	Feb	Mar	Apr	May	Jun	Jul	Aug	Sep	Oct	Nov	Dec	2010
EAS[a]	1778.1	46.4	35.6	33.0	24.1	23.9	24.0	24.0	23.6	23.5	25.0	31.4	41.0	355.6
EUR[b]	326.3	6.7	6.4	7.2	6.5	5.3	4.9	4.0	3.7	4.4	5.2	5.3	5.7	65.3
MDE[c]	26.7	0.4	0.4	0.5	0.5	0.5	0.4	0.4	0.4	0.4	0.5	0.5	0.5	5.3
NAM[d]	310.8	5.2	5.1	5.3	5.1	5.1	5.2	5.3	5.3	5.1	5.1	5.1	5.2	62.2
RBU[e]	93.0	2.0	1.9	1.9	1.7	1.4	1.3	1.0	1.1	1.2	1.6	1.7	1.8	18.6
SAS[f]	1162.7	20.4	19.1	19.7	18.9	19.2	18.9	19.2	19.2	19.0	19.3	19.2	20.4	232.5
All	3697.6	81.2	68.5	67.6	56.8	55.4	54.7	53.9	53.3	53.6	56.7	63.2	74.6	739.5
Global	5492.9	110.6	86.2	92.8	103.9	98.7	97.2	86.8	85.4	85.4	84.2	83.3	83.9	1098.6

[a] East Asia. [b] Europe. [c] Middle East. [d] North America. [e] Russia–Belarus–Ukraine. [f] South Asia.

Figure 1b–g illustrates the spatial distribution of the 20% reductions of annual BC emissions in six source regions in 2010. It can be found that the most intense reductions of BC emissions in EAS and SAS were concentrated in East China and India, respectively, which were mainly attributed to emissions from residential sectors, followed by transportation and industries. The BC emission reductions of EUR were widely distributed with high values in central Europe, with residential and transportation sectors accounting for the largest proportion. The reductions near the Arctic circle could be found in the north of EUR, NAM, and RBU. For MDE, most BC was emitted from Iran, which located in the northeast of this region. Overall, the spatial pattern of BC emission reductions in six regions was closely related to the spatial distribution of the human population.

2.1.2 Model description

Considering that the simulations should cover all months of 2010 and all emission source regions,

five global models (i.e. CAMchem, CHASER_re1, GEOS-Chem, GOCART–v5, and Oslo CTM3–v2) were incorporated to simulate the responses of BC concentrations in the Arctic to 20% BC emission reductions from EAS, EUR, MDE, NAM, RBU, and SAS, respectively. The brief information of model configurations is listed in Table 2. As required by HTAP2, all simulations should include a spin-up time of 6 months prior to the period of interest. The outputs from all models are available upon request from http://aerocom.met.no. The time resolution of the outputs used in this study is monthly for all models, although models were run at a finer resolution (e.g., daily or hourly). The model outputs for air pollutants were originally provided in the unit of mass mixing ratio (MMR, kg kg^{-1}). To facilitate comparison between model and observation and further data analysis, we converted the original units into ng m^{-3} based on the ideal gas law (Aamaas et al., 2017).

Table 2. Configurations of models used in this study

Models	Meteorological field	Horizontal resolution	Vertical layers	Convection	Reference
CAMchem	GEOS5 v5.2	1.9° × 2.5°	56	Zhang–McFarlane approach for deep convection	Lamarque et al., 2012; Tilmes et al., 2016
CHASER_re1	ERA-Interim and HadISST	2.8° × 2.8°	32	CCSR/NIES AGCM for advection, convection, and other subgrid–scale mixing	Sudo et al., 2002; Takashi et al., 2018
GEOS-Chem	GEOS–5 (MERRA)	2.0° × 2.5°	47	Convective transport is computed from the convective mass fluxes in the meteorological archive	Henze et al., 2007
GOCART–v5	MERRA	1.3° × 1.0°	72	MERRA for moist convection, Arakawa–Schubert (RAS) algorithm for GCTM	Chin et al., 2000
Oslo CTM3–v2	ECMWF–IFS	2.8° × 2.8°	60	Tiedke mass flux scheme for deep convection	Søvde et al., 2012; Lund et al., 2018

2.2 Calculation of the temperature response to BC emissions reduction

The climate effects of air pollutants have been the focus of climate change research since the last century (IPCC, 1990; IPCC, 2001). In the last few years, the metrics for estimating this kind of effect have been constantly improving (Shindell et al., 2012; Bond et al., 2013; Smith and Mizrahi, 2013; Stohl et al., 2015). The Intergovernmental Panel on Climate Change (IPCC) used the Global Warming Potential (GWP) as a method for comparing the potential climate impact of emissions of

different greenhouse gases (IPCC, 1990). GWP is the time-integrated radiative forcing due to a pulse emission of a given species, over some given time horizon (commonly 20, 100, or 500 years) relative to a pulse emission of carbon dioxide. GWP does not purport to represent the impact of air pollutant emissions on temperature. Although a short-lived climate pollutant (SLCP) could have the same GWP as a long-lived climate pollutant, identical (in mass terms) pulse emissions could cause a different temperature change at a given time, because long-lived climate pollutants accumulate in the climate system while short-lived climate pollutants can be broken down by various processes. Consequently, warming caused by long-lived climate pollutants is determined by total cumulative emissions to date, while the warming due to short-lived climate pollutants is determined more by the current rate of emissions in any given decade and depends much less on historical emissions. This means the importance of SLCP emissions is often overstated based on GWP. Shine et al. (2005) proposed the Global Temperature Change Potential (GTP) as a replacement for GWP to represent the global-mean surface temperature change for both a pulse emission (GTP_P) and a sustained change in emissions (GTP_S) of a given air pollutant. The distinction between GTP_P and GTP_S avoids the overestimation of GWP for the short-lived climate pollutants. Even for a uniform forcing, there will be differences of spatial patterns in the temperature response. Regional Temperature-change Potential (RTP) (Shindell and Faluvegi, 2010) was applied to analyze the temperature response on the regional scale, since both GWP and GTP focused on the global scale. The GWP, GTP, and RTP were normalized to the corresponding effect of CO_2 as the Absolute Global Warming Potential (AGWP), Absolute Global Temperature Change Potential (AGTP), and Absolute Regional Temperature-change Potential (ARTP), respectively. AGWP represented the absolute forms of radiative forcing. AGTP and ARTP represented the absolute forms of temperature perturbation.

ARTPs is more suitable for this study to calculate the temperature response, considering that the research object is BC with short lifetime and focus on regional impact of the BC emission reductions on temperature changes in the Arctic. For SLCFs with atmospheric lifetimes much shorter than both the time horizon of the ARTP and the response time of the climate system, the general expression for the ARTP following a pulse emission of BC (E) in region r which leads to a response in latitude band m is as follows (Fuglestvedt et al., 2010; Collins et al., 2013; Aamaas et al., 2017):

$$\mathrm{ARTP}_{r,m,s}(H) = \sum_l \frac{F_{l,r,s}}{E_{r,s}} \times \mathrm{RCS}_{l,m} \times R_T(H) \quad (1)$$

214 $F_{l,r,s}$ (in W m^{-2}) is the radiative forcing in latitude band *l* due to emission in region *r* in season *s* as
215 a function after the pulse emission $E_{r,s}$ (in Tg). Even though our estimates are based on seasonal
216 emissions, the temperature responses calculated are annual means. Shindell and Faluvegi (2009)
217 analyzed BC climate effect in four different latitudes: southern mid-high latitudes (90°S–28°S),
218 tropics (28°S–28°N), northern mid-latitudes (28°N–60°N), and the Arctic (60°N–90°N), which gives
219 a better estimate of the global temperature response as it accounts for varying efficacies with latitude.
220 The $RCS_{l,m}$ is a matrix of regional response coefficients based on the RTP concept (unitless; Collins
221 et al., 2013). As these response coefficients are normalized here, they contain no information on
222 climate sensitivity, only the relative regional responses in the different latitude bands. The global
223 climate sensitivity is included in the impulse response function R_T, which is a temporal temperature
224 response to an instantaneous unit pulse of RF (in K m^2 W^{-1}). This paper refers to the ARTP values in
225 Aamaas et al. (2017). Aamaas et al. (2017) applies two refinements of the forcing-response
226 coefficients for radiative forcing occurring in the Arctic: one for the aerosol effects in the atmosphere
227 (Shindell and Faluvegi, 2010; Lund et al., 2014) and another for the effects due to BC on snow
228 (Flanner, 2013). The ARTP in this study estimated of the direct effect in the Arctic included both the
229 direct radiative forcing from outside the Arctic and within the Arctic, while the ARTP of the
230 semi-direct effect in the Arctic was due to the semi-direct radiative forcing from outside the Arctic.
231 The contribution by radiative forcing within the Arctic to Arctic temperature changes considered the
232 vertical profile of BC concentrations as both $F_{Arctic,r,s}$ and $RCS_{Arctic,Arctic}$ have a dependence on the
233 height of the BC (Lund et al., 2014; Lund et al., 2017). The total response in the Arctic was the sum
234 of the contributions from BC forcing outside of the Arctic and inside of the Arctic.
235 Regional temperature responses at time *t* of an emission *E*(t) can be calculated with these ARTP
236 values by a convolution (Aamaas et al., 2016). The temperature response is as follows:

237 $$\Delta T_{r,m,s,t}(t) = \int_0^t E_{r,s,t}(t') \times ARTP_{r,m,s,t}(t-t')dt' \quad (2)$$

238 $\Delta T_{r,m,s,t}$ refers to the decrease of the Arctic or global surface temperature after 20, 100, or 500 years
239 to 20% BC emission reductions of six regions (namely EAS, EUR, MDE, NAM, RBU, and SAS) in
240 the framework of HTAP2 either during summer or winter in this paper.

241 # 3. Results and Discussion

242 ## 3.1 Model evaluation

243 To evaluate the model performance from all five models, the monthly simulated surface BC
244 concentrations of the BASE scenario were compared with the observations at four monitoring sites in
245 the Arctic Circle in 2010. The locations of the four sites, including Alert (82.5°N, 62.3°W) in Canada,
246 Barrow (71.3°N, 156.6°W) in Alaska, Tiksi (71.59°N, 128.92°E) in Russia, and Zeppelin (78.9°N,
247 11.9°E) in Norway, are plotted in Figure S1 in the Supporting Information.

248 Metrics (Text S1) including correlative coefficient (COR), normalized mean bias (NMB),
249 normalized mean error (NME), mean bias (MB), and mean absolute error (MAE) were selected for
250 evaluating the model performance in this study (U.S. EPA, 2007) In addition to the evaluation for
251 each single model, the multi-model ensemble mean (calculated as the average of all participating
252 models) was also evaluated. The statistical results are listed in Table 3 and Table S1. A comparison
253 between the monthly variations of simulated and observed BC concentrations is shown in Figure S2
254 (a).

255 The correlations of the simulated BC concentrations among different models were moderate to
256 high with CORs ranging from 0.33 to 0.98 (Table S1), suggesting the temporal variations of different
257 models were relatively consistent. Overall, CAMchem, GEOS-Chem, GOCART–v5, and Oslo
258 CTM3–v2 underestimated the near-surface BC (Figure S2a), which may be attributed to an
259 underestimation of BC emissions, e.g., gas flaring (Huang et al., 2014, 2015; Stohl et al., 2013) and
260 shipping emissions (Marelle et al., 2016). Also, appropriate temporal allocation of BC emissions
261 from residential combustion was another important factor governing the model performance (Stohl et
262 al., 2013). However, the simulated BC surface concentrations from CHASER_re1 were higher than
263 those of the other four models and observations (Figure S2a), which mainly due to their slow BC
264 aging-rate in remote/polar regions (Sudo et al., 2015).

265 Table 3 shows the model performances at the four Arctic sites. No single model could reproduce
266 the BC concentrations in the Arctic well, and models performed differently at different monitoring
267 sites. Relatively good agreement between the observation and models was found at Zeppelin, with
268 CORs, NME, MB, and MAE of 0.59–0.83, 38.59%–142.64%, –13.53–14.97 ng m^{-3}, and 5.40–14.97

ng m^{-3}, respectively. The best correlation (0.83) was found at Zeppelin from Oslo CTM3, while the smallest NMB (38.59%) and MAE (5.40 ng m^{-3}) were found at Zeppelin from GOCART. On the contrary, the simulated BC concentrations didn't agree so well with observations at the other three sites with even negative COR values in some models (e.g., CAMchem, and CHASER_re1), which may be explained by the uncertainties in emission inventory, the bias in the meteorological simulations, and chemical mechanisms (Miao et al., 2017; Zhang et al., 2019). All models, except Oslo CTM3, overestimated the BC concentrations in Barrow in July (Figure S2a), mainly due to the large contributions of biomass burning from Siberia in the simulations caused by overestimations of emissions and/or too little removal during transport (Sobhani et al., 2018).

The vertical profiles of simulated BC concentrations of the BASE simulation were also compared with aircraft measurements from HIAPER Pole-to-Pole Observations (HIPPO) during 24 March–16 April 2010 (Figure S2b). Different from comparison between observed and simulated BC concentrations near the surface, the vertical profiles of BC concentrations were overestimated by most models. As the aircraft ascended and descended along each flight track, BC concentrations from HIPPO varied with time, latitude, longitude, and altitude. However, most of the simulation results of HTAP2 were provided in the temporal resolution of monthly, simulation and observation results cannot be exactly matched. This partly explained the difference between the simulations and observations. In general, the model ensemble mean could capture the vertical pattern of observed BC profiles.

Although the single model didn't reproduce the BC concentrations in the Arctic well, the consistency of the model ensemble mean with the observation was improved to some extent. The NME and MAE of model ensemble mean was closer to zero compared with the single model. Therefore, the multi-model ensemble mean was used for further analysis.

Table 3 Comparison of the simulations and observations of monthly surface BC concentrations at Alert, Barrow, Tiksi, and Zeppelin in 2010.

Parameters	Sites	CAMchem	CHASER_re1	GEOS-Chem	GOCART–v5	Oslo CTM3–v2	Model ensemble mean
COR[a]	Alert	–0.24	–0.22	0.35	0.20	–0.24	–0.10
	Barrow	–0.28	–0.08	0.06	0.00	0.01	–0.06
	Tiksi	–0.19	0.05	0.50	0.48	0.41	0.11
	Zeppelin	0.72	0.59	0.80	0.76	0.83	0.73

NMB[b] (%)	Alert	–86.75	115.06	–57.81	–34.31	–92.38	–9.21
	Barrow	–38.43	104.10	–38.95	–8.18	–75.58	4.37
	Tiksi	–82.03	10.31	–69.76	–67.34	–84.82	–46.79
	Zeppelin	–79.93	142.64	–45.57	–9.81	–75.98	8.63
NME[c] (%)	Alert	86.75	151.30	66.37	70.77	92.38	74.69
	Barrow	72.07	124.44	69.50	84.20	75.58	72.12
	Tiksi	82.03	64.55	70.16	68.82	84.82	60.81
	Zeppelin	79.93	142.64	45.57	38.59	75.98	42.06
MB[d] (ng m^{-3})	Alert	–29.03	11.08	–21.41	–16.07	–30.16	–12.81
	Barrow	–22.13	15.35	–19.10	–11.12	–30.40	–9.44
	Tiksi	–55.99	–17.28	–48.51	–48.16	–56.26	–40.64
	Zeppelin	–13.53	14.97	–8.19	–3.59	–12.45	–1.44
MAE[e] (ng m^{-3})	Alert	29.03	31.05	22.85	22.23	30.16	23.56
	Barrow	29.01	28.91	26.71	30.30	30.40	25.22
	Tiksi	55.99	37.06	48.60	48.49	56.26	43.73
	Zeppelin	13.53	14.97	8.19	5.40	12.45	4.95

[a] Correlative coefficient. [b] Normalized mean bias. [c] Normalized mean error. [d] Mean bias. [e] Mean absolute error.

3.2 Near-surface BC concentrations in the Arctic

Before analyzing the responses of Arctic BC to emission reductions, it is necessary to understand the spatial-temporal distribution of BC concentrations in the Arctic region. In this study, months from May to October were defined as summer and November to April were defined as winter due to the special geographical location of the Arctic (Aamaas et al., 2017).

Spatial distributions of Arctic near surface BC concentrations in summer and winter simulated from each model are showed in Figure S4. BC simulated by CHASER_re1 showed relatively high concentrations over the whole Arctic, followed by GEOS-chem and GOCART–v5, while those simulated by Oslo CTM3–v2 and CAMchem were lower. The difference of simulated BC concentrations between land and ocean was more obvious in summer than that in winter, especially for GEOS-chem and GOCART–v5. The mean BC concentrations from the ensemble models near the surface Arctic (66–90°N) were 18.6 ng m^{-3} in summer and 16.6 ng m^{-3} in winter in 2010, respectively. Figure 2 shows that the BC concentrations over the polar sea ice region in winter were higher than that in summer. The coverage of the polar dome expanded more southward in winter (Bozem et al., 2019; Law and Stohl, 2007), allowing more BC from lower latitudinal regions to be transported into the Arctic. Turbulent exchange and deposition were reduced during winter as the meteorological conditions in the Arctic were stable and dry (Bradley et al., 1992; Bozem et al., 2019;

Law and Stohl, 2007). In addition, BC emissions in EAS, EUR, and RBU regions showed obvious monthly changes with higher emissions from November to March as mentioned earlier (Section 2.1.1), leading to the relatively high BC concentrations over the polar sea ice region in winter. Over the terrestrial areas within the Arctic Circle, summer BC concentrations were higher than winter, especially in Siberia and Alaska, which were attributed to intense BC emissions from biomass burning over these areas from Jun to Aug (Figure S3).

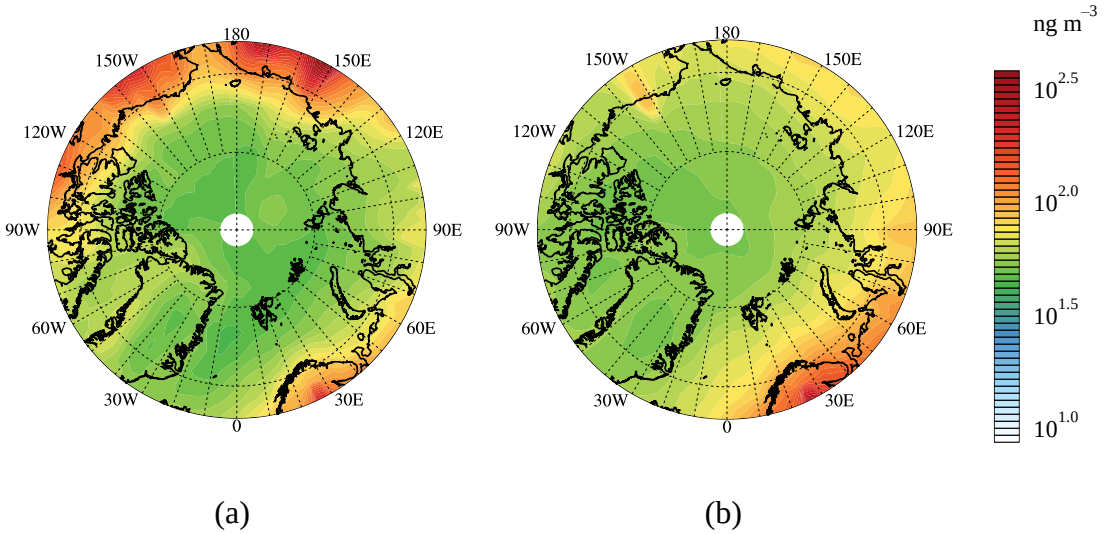

Figure 2. Spatial distribution of near-surface BC concentrations in **(a)** summer and **(b)** winter in the Arctic in 2010.

3.3 Response of Arctic BC to 20% emission reductions

3.3.1 Contributions of regional emission reductions to the Arctic near-surface BC

The response of the Arctic near-surface BC to 20% emission reductions from different source regions was analyzed through emission perturbation simulations. Figure 3 shows the spatial distribution of the referred response above in summer and in winter of 2010 based on multi-model ensemble mean results. The source region contributions to the surface BC concentrations exhibited significant seasonal variability with higher values in winter. The BC emission reductions in EAS almost affected the whole Arctic, especially in winter, indicating the significance of the intercontinental transport of BC. The spatial distribution of the Arctic near-surface BC response to SAS emission reductions was similar to that of EAS, but the extent was much weaker. The emission reductions from EUR, NAM,

and RBU mainly affected the local and nearby areas, which was generally consistent with the spatial pattern of emissions (Figure 1). The contribution from MDE emission reductions was very little.

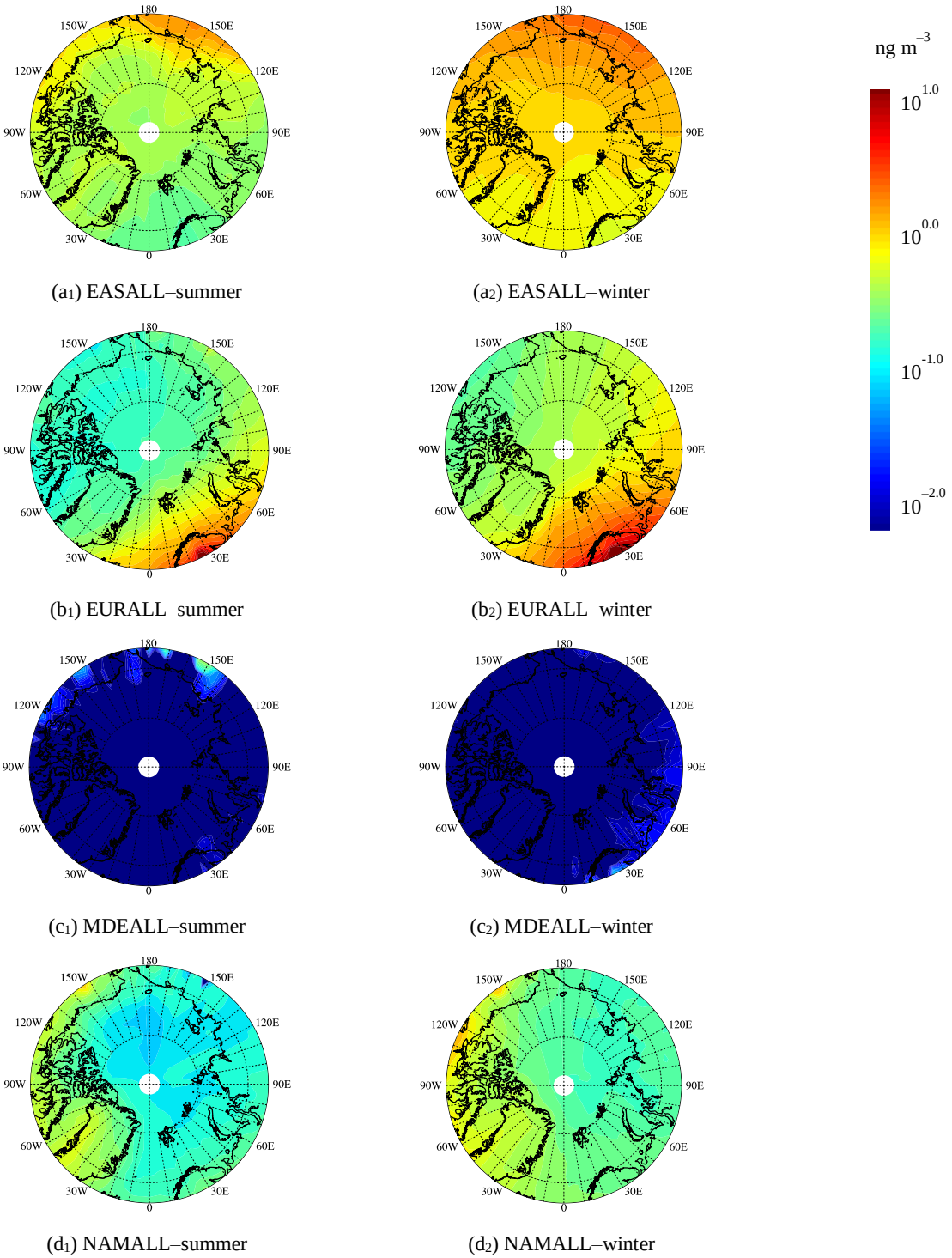

(a_1) EASALL–summer

(a_2) EASALL–winter

(b_1) EURALL–summer

(b_2) EURALL–winter

(c_1) MDEALL–summer

(c_2) MDEALL–winter

(d_1) NAMALL–summer

(d_2) NAMALL–winter

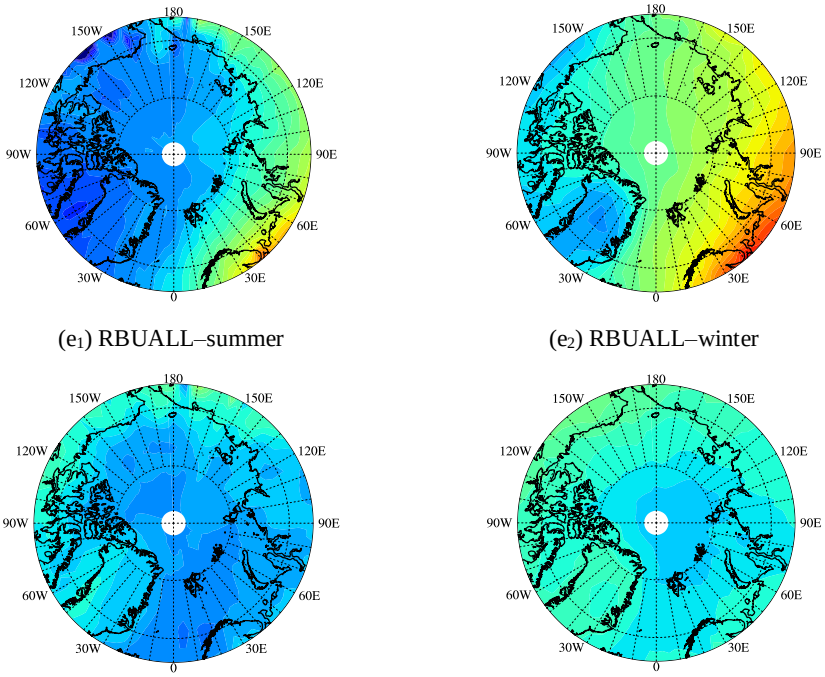

(e_1) RBUALL–summer (e_2) RBUALL–winter

(f_1) SASALL–summer (f_2) SASALL–winter

335 **Figure 3.** Spatial distribution of contribution of 20% emission reductions of different source regions to Arctic
336 near-surface BC in summer and in winter in 2010.

337 The monthly variations of the response of the Arctic near-surface BC concentrations to 20%
338 emission reductions from six source regions are presented in Figure 4. Results from the ensemble
339 simulations are averaged over the Arctic covering latitudinal areas from 66°N to the north pole. The
340 emission reductions from the total six source regions were 329.6 Gg during May to October, lower
341 than that of 411.9 Gg during November to April (Table 1). Correspondingly, the contributions of 20%
342 BC emission reductions from all six regions to Arctic near-surface BC concentrations were 0.8–1.4
343 ng m^{-3} during May to October and 1.5–3.2 ng m^{-3} during November to April. Arctic sensitivities
344 (Arctic concentration change per unit source region emission change) for BC typically maximized
345 from December to February for EUR and RBU and from March to May for EAS and NAM (Shindell
346 et al., 2008; AMAP, 2008). The enhanced sensitivity from December to May resulted from faster
347 transport and slower removal during winter as the meteorological conditions in the Arctic were stable
348 and dry (Law and Stohl, 2007). The results of deposition changes also proved this result well (Figure
349 S5). The wet deposition in summer was higher than that in winter, which was 7–13 times of dry
350 depositions. Sharma et al. (2013) found that the Arctic region (north of 70°N) was very dry during
351 winter with an average daily precipitation rate between 0 and 1 mm day^{-1}. Precipitation rates over
352 some of the BC source regions such as Eurasia were at the same order of magnitude as the Arctic.

Less wet deposition and a shallow boundary layer resulted in higher BC concentrations near the surface during winter. In the summertime, the Arctic region experienced 2 to 3 times higher precipitation rates as well as wet depositions of BC relative to wintertime, thus resulting in lower contributions to the near-surface BC concentrations.

The annual contribution of 20% emission reductions from EAS, EUR, MDE, NAM, RBU, and SAS to the Arctic near-surface BC concentrations reached 0.70, 0.54, 0.01, 0.20, 0.29, and 0.09 ng m^{-3} in 2010, respectively. Correspondingly, the annual reduced column BC loadings over the Arctic were 8521.7, 2789.1, 28.8, 1762.1, 998.6, and 3640.2 ng m^{-2} in 2010, respectively.

The response of Arctic near-surface monthly BC concentration was found strongest to the 20% emission reductions from EAS with the contribution of 0.2–1.5 ng m^{-3}, accounting for 16.8%–49.0% of the total reduced BC concentrations resulting from all six source regions (Figure 4). On one hand, the BC emission reductions in EAS were the largest among the six source regions (Table 1). On the other hand, BC emission reductions in EAS can influence the Arctic lower troposphere via two pathways (Bozem et al., 2019; Stohl, 2006). BC from northern regions of EAS can enter into the polar dome of the Arctic in winter, as the air masses have cooled during transport. BC from eastern regions of EAS fast uplifted due to convection and then followed by high altitude transport in northerly directions. Radiative cooling eventually led to a slow descent into the polar dome area after air masses arrived in the high Arctic. It occurred both in summer and winter. In addition to EAS, BC emission reduction from EUR also showed significant impacts on the Arctic near-surface monthly BC concentration with the contribution of 0.2–1.0 ng m^{-3}, accounting for 20.1%–49.0% of the total reduced BC concentrations resulting from all six source regions (Figure 4). Among the three regions in the Arctic Circle (i.e. EUR, NAM, and RBU), EUR region had the largest BC emission reductions. Also, the relatively short distance between EUR and the Arctic made EUR the second most important source region to the Arctic. As for NAM and RBU, their 20% emission reductions induced moderate reductions of the monthly Arctic near-surface BC concentrations by 0.1–0.3 and 0.1–0.7 ng m^{-3}, respectively. The contribution of 20% emission reductions from SAS to the Arctic near-surface BC concentrations was much lower of 0.0–0.2 ng m^{-3} as a significant portion of BC originating from SAS accumulated in the upper troposphere (Section 3.3.2). Compared to the five source regions discussed above, the response of Arctic BC concentrations to emission reductions from MDE was negligible, owing largely to the low emissions there and long distance from the Arctic.

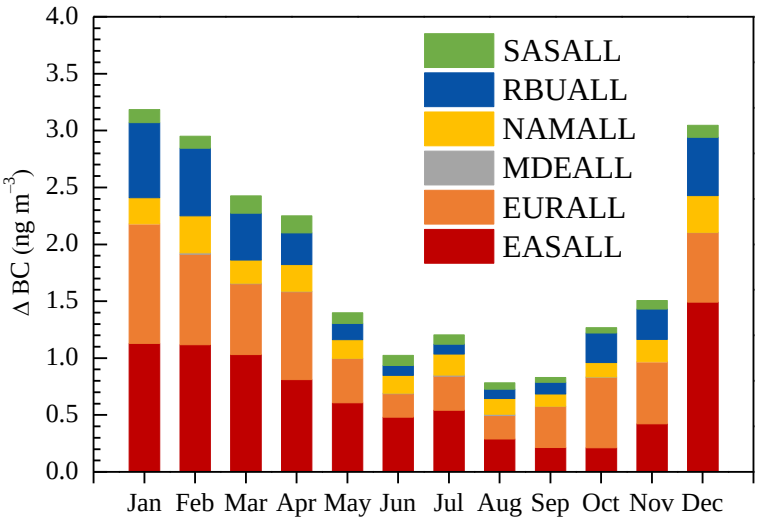

Figure 4. Monthly mean reduced concentrations of the near-surface Arctic BC due to 20% emission reductions from six source regionsin 2010.

Figure S6 compares the contributions of 20% emission reductions to Arctic near surface BC concentrations simulated by different models. All five models showed similar monthly variations, of which CHASER_re1 simulated high BC concentrations compared to the other models due to slow aging-speed (Sudo et al., 2015). All models showed the major source regions of Arctic BC from EAS, EUR, and RUB. NAM and SAS contributed moderately while the contribution from MDE was negligible.

3.3.2 Contributions of regional emission reductions to the vertical BC profiles

To assess the contributions from various source regions to the BC profiles based on the model ensemble mean, the vertical stratification needed to be unified as most participating models had different vertical settings. Since CHASER had a relatively coarse vertical resolution of 32 layers, the other models were unified to the same vertical stratification, as detailed in Table S2.

As shown in Figure 5, the contributions of regional emission reductions to BC exhibited strong vertical gradients over the Arctic. In general, the BC profiles displayed a bimodal pattern in summer, showing peaks at around 1.0–1.6 km a.s.l. (4th and 5th layers) and 8.0–8.9 km a.s.l. (13th and 14th layers). While in winter, the BC profiles showed a unimodal pattern with peaks around 0.6–1.6 km a.s.l. (3rd – 5th layers). Long-range transport of air pollutions may occur near the planetary boundary layer (Eckhardt et al., 2003; Stohl et al., 2002). High contributions in the low layers (e.g., 3rd – 5th

layers) were consistent with the height of the planetary boundary layer in the Arctic (Zhang, et al., 2018; Cheng, 2011).

It has been summarized that there were several major transport pathways for BC into the Arctic troposphere (Stohl, 2006). i) BC transported rapidly at low-level, followed by uplifting at the Arctic front when it is located far north. Significant deposition of BC in the Arctic occurs mostly north of 70°N for this transport route. This transport route derived often from the high BC emission areas in northern EUR but seldom from the NAM and RBU. That was mainly due to that the BC emissions exist at high enough latitudes in EUR, which can be north of the polar front. However, the BC emissions in NAM and RBU were concentrated south of the polar front (Figure 1), thus BC emitted from these two regions can't be easily transported into the Arctic through this pathway. ii) Cold air masses into the polar dome transport at low-level. This pathway derived mainly from EUR and high-latitude areas of EAS during winter. The contribution of 20% emission reductions from EUR to the Arctic BC concentrations peaked at around 1.0 km a.s.l. with the multi-model ensemble mean value of 0.4 ng m^{-3} in summer, while peaked at lower altitude of around 1.6 km a.s.l. with the value of 0.8 ng m^{-3} in winter. iii) BC could also ascend south of the Arctic followed either by high–altitude transport or by several cycles of upward and downward transport, and finally slowly descended into the polar dome due to radiative cooling. This was the frequent transport route from source regions such as NAM, RBU, and east EAS. The contribution from NAM and RBU to the Arctic BC peaked at about 1.6 km a.s.l. (0.2 ng m^{-3}) and 1.0 km a.s.l. (0.2 ng m^{-3}) in summer, and peaked at about 1.0 km a.s.l. (0.3 ng m^{-3}) and 0.4 km a.s.l. (0.5 ng m^{-3}) in winter. The contribution from EAS including pathways ii and iii, to the Arctic BC peaked at about 1.6 km a.s.l. (0.6 ng m^{-3}) in summer and peaked at about 2.4 km a.s.l. (1.6 ng m^{-3}) in winter. The contribution from MDE was negligible.

As shown in Figure 5, BC can also be transported into the upper troposphere of the Arctic. Air masses preferably kept their potential temperature almost constant during transport as the atmospheric circulation can be well described by adiabatic motions in the absence of diabatic processes related to clouds, radiation, and turbulence. The potential temperature was low within the polar dome area, and thus only air masses experienced diabatic cooling were able to enter the polar dome (Stohl, 2006). That is to say, the air masses from SAS and low-latitude regions of EAS were not easy to penetrate the polar dome but can be lifted and transported to the Arctic in the middle and upper troposphere along the isentropes (AMAP, 2011; Barrie, 1986; Law and Stohl, 2007; Stohl,

2006). This agreed well with the previous study of Koch and Hansen (2005) and Stohl (2006). The contribution from SAS to the Arctic BC concentrations peaked at about 9.7 km a.s.l. (0.4 ng m^{-3}) in summer and 9.7 km a.s.l. (0.5 ng m^{-3}) winter. This was also consistent with the vertical profiles of BC shown in Stjern et al. (2016). The polar dome boundary was variable in time and space and was not zonally symmetric. The range of polar dome expanded southward to about 40°N over Eurasia in winter as the temperature difference of different latitudes became smaller (Bozem et al., 2019; Law and Stohl, 2007), resulting in the contribution of EAS to the Arctic BC concentrations in upper troposphere only peak in summer at 13th layer (8.0 km a.s.l.) with the value of 0.6 ng m^{-3}.

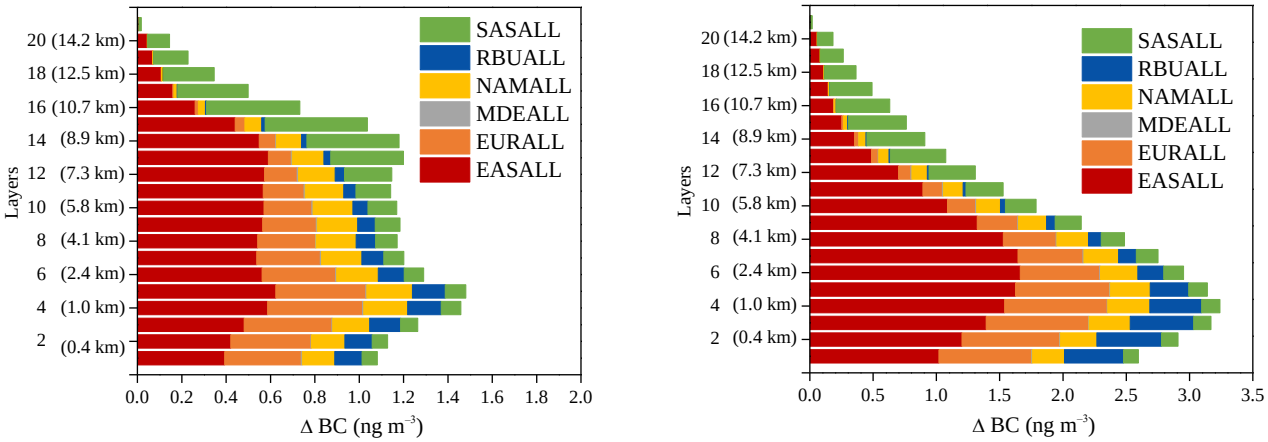

Figure 5. Contribution of 20% emission reductions from six source regions to BC concentrations in different vertical layers **(a)** in summer and **(b)** in winter in the Arctic in 2010.

3.3.3 Contributions of emission reductions to BC in different latitudinal bands

To further analyze the response of the Arctic BC concentrations to emission reductions of six source regions in HTAP2, the contribution of 20% emission reductions to BC concentrations at different latitudes of the Arctic were calculated (Figures 6 and 7). In regard to the different horizontal resolution of participating models, the Arctic region (66–90°N) was divided into eight latitudinal bands with a 3–degree interval, which was based on the coarsest resolution of all models.

The response of the Arctic BC concentrations to emission reductions of six source regions became weaker with the increase of the latitude due to the continuous loss of BC during transport (e.g., dry and wet depositions) (Figure 6). The difference of contributions between two adjacent latitudinal bands became smaller as closer to the north pole. The contributions of 20% emission reductions to

the Arctic BC concentrations near surface were the highest between 66–69°N both in summer (1.9 ng m^{-3}) and winter (4.1 ng m^{-3}), which were 1.4–2.8 times higher than the other latitudinal bands.

The contributions from EAS and EUR were higher than those from the other four regions in each latitudinal band. In detail, the contributions from EUR (0.8 ng m^{-3} in summer and 1.5 ng m^{-3} in winter) were higher than those from EAS (0.6 ng m^{-3} in summer and 1.2 ng m^{-3} in winter) in the latitudinal band of 66–69°N as the BC concentrations near surface there were more sensitive to the local emission sources. In contrast, the contributions from EAS (0.3–0.4 ng m^{-3} in summer and 0.9–1.1 ng m^{-3} in winter) were higher than those from EUR (0.2–0.4 ng m^{-3} in summer and 0.4–0.9 ng m^{-3} in winter) in the other high latitudinal bands where long-range transport played the dominant role.

The downward trends of the response of the Arctic near surface BC to emission reductions with the increase of latitude from EUR and RBU were more obvious than that of other regions (Figure 6). Dry and wet depositions of BC decreased with the increase of transport distance, and the decreasing rates became slower (Figure S7). The changes of dry and wet depositions caused by emission reductions from EUR and RBU were still obvious in the Arctic region (66°N–90°N), while depositions caused by emission reductions from the other regions tended to be gentle (Figure S7). This explains why the contribution from EAS to BC at different latitudes remained almost constant while that from EUR and RBU decreased obviously from lower latitudes to the Arctic pol

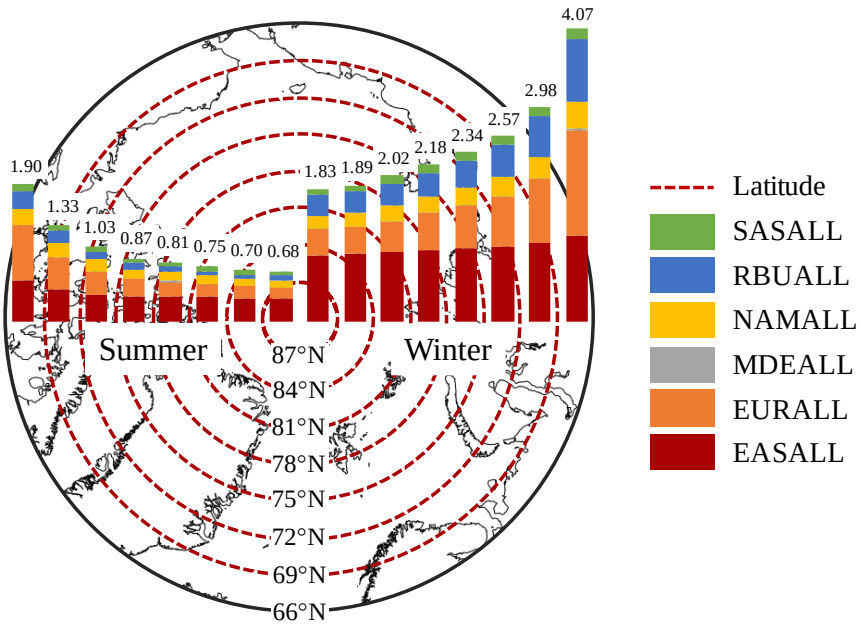

Figure 6. Contributions of 20% emission reductions of different regions to near-surface BC concentrations in each latitudinal band of the Arctic. The results of summer and winter correspond to the left and right panel in the figure.

Figure 7 further depicts the response of the vertical Arctic BC profiles in different latitudinal bands to 20% emission reductions. The contributions of eight latitudinal bands showed a typical bimodal pattern in summer with peaks at 0.6–1.6 km a.s.l. (3^{rd} – 5^{th} layers) and 8.0–8.9 km a.s.l. (13^{th} and 14^{th} layers), while the contribution displayed a single peak at the 0.4–1.0 km a.s.l. (2^{nd} – 4^{th} layers) in winter. Similar to section 3.3.2, the peak value of the contribution at the low layers was due to the transport of EAS, EUR, NAM, and RBU emission reductions to the Arctic through different pathways both in summer and winter. The peak value in the high layers in summer was due to the transport of EAS and SAS. However, a high contribution of 20% emission reductions to BC concentrations in SAS was found in the high layers, while the contribution was low in other regions, leading to a single peak in winter. The statistical results of SAS indicated that the contribution in vertical appeared one peak at the 15^{th} layer (9.7 km a.s.l.) with a value of 0.45–0.48 ng m^{-3} in summer and winter (Figure S8).

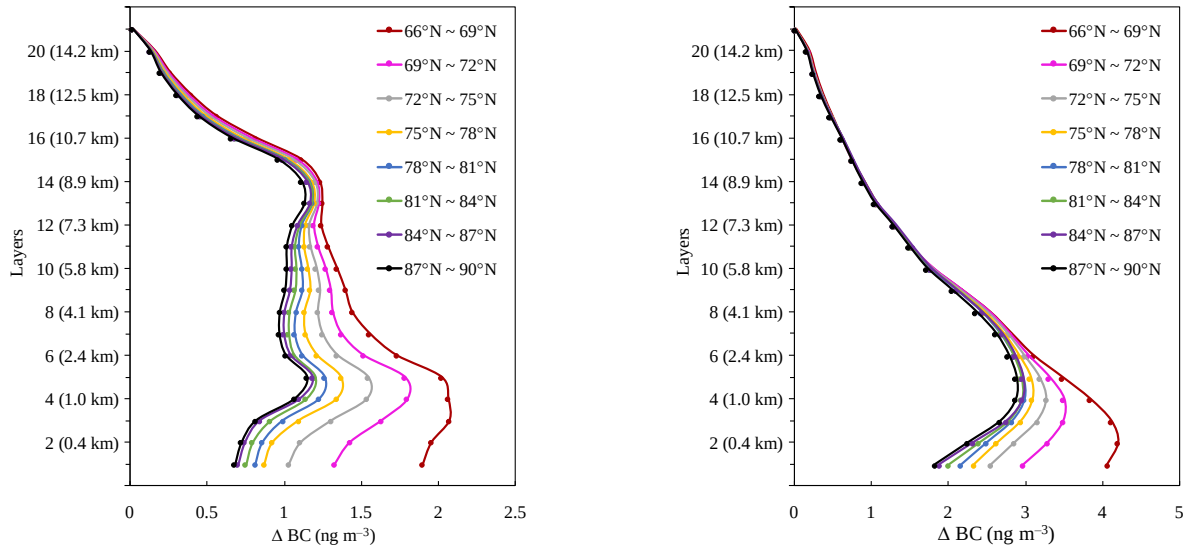

Figure 7. Contributions of 20% emission reductions from all six source regions to the vertical BC concentrations of the Arctic in different latitude bands varies with vertical layers in **(a)** summer and **(b)** winter in 2010.

As same as the whole Arctic region (Section 3.3.1 & 3.3.2), the contributions of 20% emission reductions to BC concentrations in eight latitude bands were higher in winter than in summer, whether near surface or in vertical. The contribution of 20% emission reductions from all six source regions to BC concentrations in eight latitude bands of the Arctic near surface was 0.7–1.9 ng m^{-3} in

summer and 1.8–4.1 ng m^{-3} in winter, respectively (Figure 6). The high BC peak at around 0.6–1.6 km a.s.l. (3^{rd} – 5^{th} layers) was 1.1–2.1 ng m^{-3} in summer, and 2.9–4.2 ng m^{-3} in winter (Figure 7).

3.4 Benefit of BC emission reductions on the decrease of Arctic temperature

The impact of BC emission reductions on decreasing the Arctic (60–90°N) surface temperature was assessed by using ARTP (See methods in Section 2.2). Aerosol effects, BC deposition on snow, and BC semi-direct were considered in the calculation of ARTP (Aamaas et al., 2017). As shown in Figure 8, the response of Arctic surface temperature to emission reductions was the most significant at the time scale of 10 years and then gradually decreased with the passage of time. For each source region, the Arctic temperature response was significantly higher in winter than in summer as ARTP was seasonal dependent with higher values in the colder seasons. Obviously, the Arctic surface temperature benefited the most from BC emission reductions from EAS with more than 300 and 660 μK decreases in summer and winter after 10 years, respectively. The influences of EUR and NAM emission reductions on the temperature decrease were similar in summer, reaching about 3–90 μK after 10, 20, 50, and 100 years. However, in winter, the influence of emission reductions from NAM on temperature decrease (8–200 μK) was weaker than that from EUR (14–370 μK). This was mainly due to the difference of ARTPs between EUR and NAM was not obvious compared with the difference of emission reductions from NAM and EUR in summer and winter. The responses of the temperature decrease to emission reductions from RBU were 9–20 μK in summer and 4–100 μK in winter after 10-100years, respectively, which were smaller than that from EUR and NAM. This can be explained by the low BC emission reductions from RBU (Table 1). The response of the temperature decrease to emission reductions from SAS in winter (10–320 μK) was similar to that from EUR, while this response in summer (8–230 μK) was more than twice that of EUR. Although the ARTP of EUR was higher than that of SAS, the BC emission reductions from SAS were much higher than that from EUR and the difference between emission reductions from the two regions was more obvious in summer (Table 1). In spite of the higher Arctic temperature response to EAS than SAS in the target year of this study, a number of studies have shown that BC emissions in South Asia were increasing in recent years (Sahu et al., 2008; Paliwal et al., 2016; Sharma et al., 2019) while the emissions of East Asia were exhibiting a downward trend especially from China (Chen et. al., 2016), thus it should be given more attention to the impact assessment of South Asia on the Arctic in the

future. The minimum temperature response was found from MDE due to the least emission reductions and small ARTP.

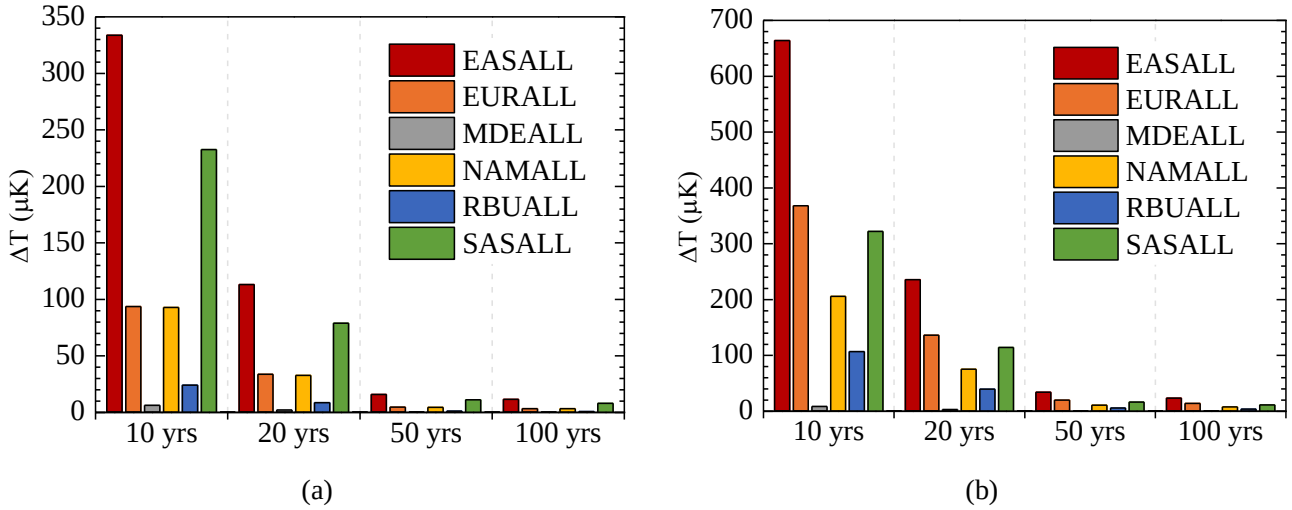

Figure 8. Arctic surface temperature response to 20% regional BC emission reductions in **(a)** summer and **(b)** winter after 10, 20, 50, and 100 years.

In addition, the impacts of BC emission reductions from six source regions on the Arctic and global surface temperature were compared in this study (Figure 9). Due to the BC emission reductions from the six source regions, the surface temperature in the Arctic decreased 27–780 μK in summer and 61–1675 μK in winter after 10, 20, 50, and 100 years, which were higher than that of the global with the values of 10–290 μK in summer and 16–470 μK in winter. It can be seen that the difference of the temperature response between the Arctic and the globe was more obvious in winter. Overall, the response of the Arctic surface temperature was more sensitive to emissions perturbation than that of the globe surface temperature.

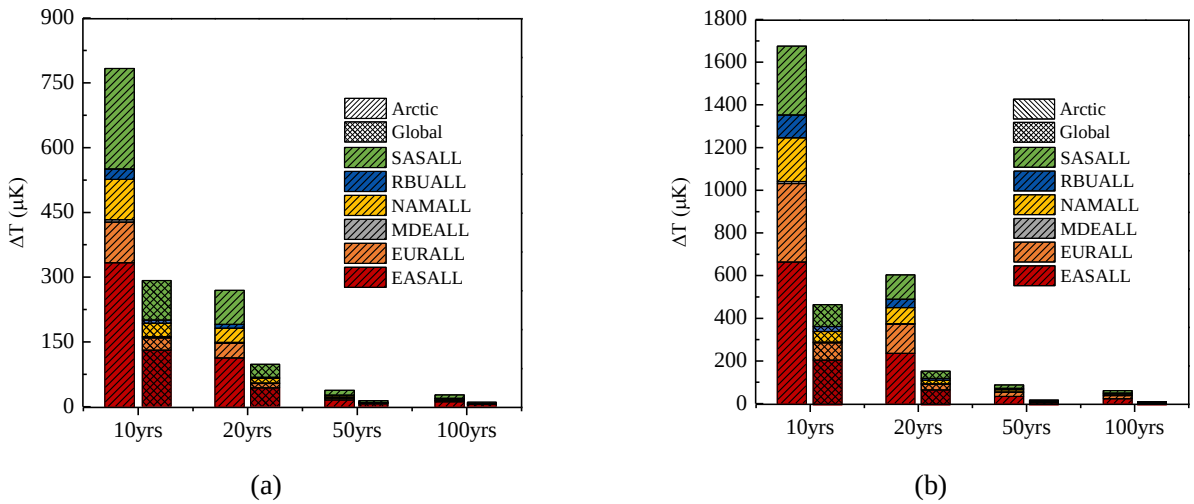

Figure 9. Global and Arctic surface temperature responses to 20% regional BC emission reductions in **(a)** summer and **(b)** winter after 10, 20, 50, and 100 years.

It should be noted the estimation of temperature response was subject to large uncertainties for the following reasons. On the one hand, even though the HTAP2 emissions database were all constructed by bottom-up methods, the different inventories and spatiotemporal distributions were constructed with sub-regional (country, state, county or province level) activity data and emission factors, which lead to inconsistencies at the borders between two adjacent inventories. The version 5 of Evaluating the Climate and Air Quality Impacts of Short-Lived Pollutants (ECLIPSEv5, http://eclipse.nilu.no) estimated a 2010 emission inventory, that serves also as a reference point for all projections (Janssens-Maenhout et al., 2015). At the global level, a relatively good agreement was found with small relative emission differences compared with the ECLIPSEv5 emission inventory for the aggregated sectors in 2010. However, larger differences of 29% between HTAP2 and ECLIPSEv5 emissions was present for BC since ECLIPSEv5 relied on provincial statistics for China which resulted from higher coal consumption than reported national statistics. Hoesly et al. (2018) provided a sectoral and gridded historical (1750–2014) anthropogenic emission inventory for use in the Coupled Model Intercomparison Project phase 6 (CMIP6). The amount of global BC anthropogenic emissions was 7.7 Tg/year in 2010 from the CMIP6 emissions, which was larger than that from HTAP2 emissions (5.5 Tg/year). This was mainly due to the energy, transportation, and international shipping sectors of CMIP6 were higher than those of HTAP2.

On the other hand, the time evolution of R_T, a parameter in the calculation of ARTP was also one factor causing the uncertainty of temperature response calculation. This impulse response function was only based on one coupled atmosphere-ocean climate model GISS-ER in this study, while Olivié and Peters (2013) have found a spread in the GTP (20) value of BC of about −60 to +80% due to variability of R_T among various models. However, the uncertainty in R_T was less relevant for the regional patterns. Forcing-response coefficients didn't exist on a seasonal basis since emissions occurring during Northern Hemisphere summer and winter season were differentiated (Aamaas et al, 2017). Hence, the seasonal differences presented here in the ARTP values were not due to potential differences in the response sensitivities, but due to differences in the RF. The temperature response will vary by species and location, such as between land surface and ocean surface. These differences are not accounted for in this study, but the increased efficacy in the RCS matrix towards the NH can

be partly attributed to a larger land area fraction in the NH (Shindell et al., 2015). Besides, recent studies have found that the positive radiation budget of BC being largely compensated for by rapid atmospheric adjustment, this means that the responses of surface temperatures to BC tends to be weaker than expected (Stjern et al., 2017; Takemura and Suzuki, 2019).

Although the HTAP2 emissions database contain uncertainties and ARTP calculations are simplifications, these emission metrics are useful, simple, and quick approximations for calculating the temperature response in the different latitude bands for emissions of BC.

4. Conclusions

The CAMchem, CHASER_re1, GEOS-Chem, GOCART, and Oslo CTM3 in HTAP2 experiment were used in this study to estimate the responses of Arctic BC to multi-region emission reductions in 2010. Six regions (e.g., EAS, EUR, MDE, RBU, NAM, and SAS) were selected as the source regions and the Arctic was the receptor region. HTAP2 set up the base scenario with all BC emissions, and also simulated BC concentrations with 20% reduction of anthropogenic emissions. The AGPT was further used to calculate the benefit of BC emission reductions on the decrease of Arctic temperature.

The statistical results of 20% BC emission reductions showed that emission reductions in EAS were the largest with the values of 355.6 Gg yr^{-1}, followed by SAS (232.5 Gg yr^{-1}), EUR (65.3 Gg yr^{-1}), NAM (62.2 Gg yr^{-1}), RBU (18.6 Gg yr^{-1}), and MDE (5.3 Gg yr^{-1}). The BC emission reductions in the EAS, EUR, and RBU were higher from November to March.

The temporal variations of simulations from different models were relatively consistent as the correlations of the simulated BC concentrations among different models ranged from 0.33 to 0.98. However, the simulated BC concentrations didn't agree so well with observations at monitoring sites except Zeppelin. In order to reduce the difference of simulation performance of each model in different areas of the Arctic, the model ensemble mean was used for analysis.

The contribution of 20% BC emission reductions from EAS, EUR, MDE, NAM, RBU, and SAS to the Arctic near-surface BC concentrations reached 0.70, 0.54, 0.01, 0.20, 0.29, and 0.09 ng m^{-3}, respectively. Correspondingly, the reduced column BC loadings from the six regions above over the Arctic was 8521.7, 2789.1, 28.8, 1762.1, 998.6, and 3640.2 ng m^{-2}, respectively.

The response of Arctic near-surface BC concentrations to 20% emission reductions from EAS and EUR was larger than other four source regions, with the monthly value of 0.2–1.5 ng m^{-3} and 0.2–1.0 ng m^{-3}, accounting for 16.8%–49.0% and 20.1%–49.0% of the total contributions from all six regions, respectively. The BC profiles displayed a bimodal pattern in summer with peaks at around 1.0–1.6 km a.s.l. (4^{th} and 5^{th} layers) and 8.0–8.9 km a.s.l. (13^{th} and 14^{th} layers). While the BC profiles showed a unimodal pattern with peaks around 0.6–1.6 km a.s.l. (3^{rd} – 5^{th} layers) in winter.

The response of Arctic BC to emission reductions from source regions in winter was higher than that in summer. The contributions of 20% emission reductions to the Arctic BC concentrations near surface were the highest between 66–69°N both in summer (1.9 ng m^{-3}) and winter (4.1 ng m^{-3}), and became weaker with the increase of the latitude.

The response of Arctic temperature to BC emission reductions was the most significant at the time scale of 10 years and then gradually decreased with the passage of time. The Arctic had benefited the most from emission reduction in EAS with more than 300 and 660 μK decreases in summer and winter after 10 years, respectively. The Arctic temperature response was more sensitive to the whole globe in regard of the same emissions perturbation. The estimation of temperature response was subject to large uncertainties due to the uncertainties in the calculation of ARTP and emissions of BC in source regions.

Overall, this study provided insights on the source regions and seasonal contributions of Arctic BC from the most recent international ensemble modeling efforts. The discrepancy between model results and observations and the spread among different HTAP models may be attributed to various factors such as emissions in the remote Arctic, physical parameterizations, and convection and deposition processes. This would subsequently result in large uncertainties of the climatic effects of air pollutants. More observation sites on the typical transport pathways from sources regions to the Arctic should be planned to improve the model capability of simulating the transport behavior of black carbon.

Data availability

All data used in this paper can be obtained through the AeroCom servers and web interfaces, accessible at http://aerocom.met.no.

Author contributions

KH and JSF designed this study. ML, KS, DH, TK, MC, and ST performed modeling. NZ analyzed data and wrote the paper. All have commented on and reviewed the paper.

Competing interests.

The authors declare that they have no conflict of interest.

Acknowledgements

We sincerely thank for the HTAPv2 international initiative. This work was partially supported by the National Natural Science Foundation of Shanghai (18230722600), the National Key R&D Program of China (2018YFC0213105), and the National Natural Science Foundation of China (91644105).

References

Aamaas, B., Berntsen, T. K., Fuglestvedt, J. S., Shine, K. P., and Bellouin, N.: Regional emission metrics for short–lived climate forcers from multiple models, Atmos. Chem. Phys., 16, 7451– 7468, https://doi.org/10.5194/acp–16–7451–2016, 2016.

Aamaas, B., Berntsen, T. K., Fuglestvedt, J. S., Shine, K. P., and Collins, W. J.: Regional temperature change potentials for short-lived climate forcers based on radiative forcing from multiple models, Atmos. Chem. Phys., 17, 10795-10809, 10.5194/acp-17-10795-2017, 2017.

AMAP: Black carbon and ozone as Arctic climate forcers. Arctic Monitoring and Assessment Programme (AMAP), Oslo, Norway. vii + 116 pp, 2015.

AMAP: Snow, Water, Ice and Permafrost in the Arctic (SWIPA) 2017. Arctic Monitoring and Assessment Programme (AMAP), Oslo, Norway. xiv + 269 pp. ISBN 978–82–7971–101–8, 2017.

AMAP: The Impact of Black Carbon on Arctic Climate. By: Quinn, P. K., Stohl, A., Arneth, A., Berntsen, T., Burkhart, J. F., Christensen, J., Flanner, M., Kupiainen, K., Lihavainen, H., Shepherd, M., Shevchenko, V., Skov, H., and Vestreng., V., Arctic Monitoring and Assessment Programme (AMAP), Oslo. 72 pp, 2011.

AMAP: The Impact of Short–Lived Pollutants on Arctic Climate. By: Quinn, P. K., Bates, T. S., Baum, E., Bond, T., Burkhart, J. F., Fiore, A. M., Flanner, M. G., Garrett, T., Koch, D., Mcconnell, J. R., Shindell, D., and Stohl, A., Arctic Monitoring and Assessment Programme (AMAP), Oslo, Norway, 2008.

Barrie, L. A.: Arctic air pollution: an overview of current knowl- edge, Atmos. Environ., 20, 643–663, 1986.

Bond, T. C., Doherty, S. J., Fahey, D. W., Forster, P. M., Berntsen, T., DeAngelo, B. J., Flanner, M. G., Ghan, S., Kärcher, B., Koch, D., Kinne, S., Kondo, Y., Quinn, P. K., Sarofim, M. C., Schultz, M. G., Schulz, M., Venkataraman, C., Zhang, H., Zhang, S., Bellouin, N., Guttikunda, S. K., Hopke, P. K., Jacobson, M. Z., Kaiser, J. W., Klimont, Z., Lohmann, U., Schwarz, J. P., Shindell, D., Storelvmo, T., Warren, S. G., and Zender, C. S.: Bounding the role of black carbon in the climate system: A scientific assessment, J. Geophys. Res.–Atmos., 118, 5380–5552, https://doi.org/10.1002/jgrd.50171, 2013.

Bozem, H., Hoor, P., Kunkel, D., Köllner, F., Schneider, J., Herber, A., Schulz, H., Leaitch, W. R., Aliabadi, A. A., Willis, M. D., Burkart, J., and Abbatt, J. P. D.: Characterization of transport regimes and the polar dome during Arctic spring and summer using in situ aircraft measurements, Atmos. Chem. Phys., 19, 15049-15071, 10.5194/acp-19-15049-2019, 2019.

Bradley, R. S., Keimig, F. T., and Diaz, H. F.: Climatology of surface-based inversions in the North American Arctic, J. Geophys. Res., 97, 15 699, https://doi.org/10.1029/92JD01451, 1992.

Chen, D. S., Zhao, Y. H., Nelson, P., Li, Y., Wang, X. T., Zhou, Y., Lang, J. L., and Guo, X. R.: Estimating ship emissions based on AIS data for port of Tianjin, China. Atmos. Environ. 145: 10–18. http://dx.doi.org/10.1016/j.atmosenv.2016.

Cheng, G.: Analysis of observational data of atmospheric boundary layer characteristics in the Arctic (in Chinese), Nanjing University of information engineering. 2011.

Chin, M., Rood, R. B., Lin, S.–J., Müller, J.–F., and Thompson, A. M.: Atmospheric sulfur cycle simulated in the global model GOCART: Model description and global properties, J. Geophys. Res.–Atmos., 105, 24671–24687, doi:10.1029/2000JD900384, 2000.

Clarke, A. D. and Noone, K. J.: Soot in the Arctic snowpack: a cause for perturbations in radiative transfer, Atmos. Environ., 19, 2045–2053, https://doi.org/10.1016/0004-6981(85)90113-1, 1985.

Collins, W. J., Fry, M. M., Yu, H., Fuglestvedt, J. S., Shindell, D. T., and West, J. J.: Global and regional

temperature-change potentials for near-term climate forcers, Atmos. Chem. Phys., 13, 2471-2485, 10.5194/acp-13-2471-2013, 2013.

Eckhardt, S., Stohl, A., Beirle, S., Spichtinger, N., James, P., Forster, C., Junker, C., Wagner, T., Platt, U., and Jennings, S. G.: The North Atlantic Oscillation controls air pollution transport to the Arctic, Atmos. Chem. Phys., 3, 1769–1778, https://doi.org/10.5194/acp–3–1769–2003, 2003.

Flanner, M. G.: Arctic climate sensitivity to local black carbon, J. Geophys. Res.-Atmos., 118, 1840–1851, https://doi.org/10.1002/jgrd.50176, 2013.

Fuglestvedt, J. S., Shine, K. P., Berntsen, T., Cook, J., Lee, D. S., Stenke, A., Skeie, R. B., Velders, G. J. M., and Waitz, I. A.: Transport impacts on atmosphere and climate: metrics, Atmos. Environ., 44, 4648–4677, https://doi:10.1016/j.atmosenv.2009.04.044, 2010.

Galmarini, S., Koffi, B., Solazzo, E., Keating, T., Hogrefe, C., Schulz, M., Benedictow, A., Griesfeller, J. J., Janssens-Maenhout, G., Carmichael, G., Fu, J., and Dentener, F.: Technical note: Coordination and harmonization of the multi-scale, multi-model activities HTAP2, AQMEII3, and MICS-Asia3: simulations, emission inventories, boundary conditions, and model output formats, Atmos. Chem. Phys., 17, 1543–1555, 2017.

Garrett, T. J. and Zhao, C.: Increased Arctic cloud longwave emissivity associated with pollution from mid-latitudes, Nature, 440, 787–789, 2006.

Hansen, J. and Nazarenko, L.: Soot climate forcing via snow and ice albedos, P. Natl Acad. Sci. USA, 101, 423–428, https://doi.org/10.1073/pnas.2237157100, 2004.

Henze, D. K., Hakami, A., and Seinfeld, J. H.: Development of the adjoint of GEOS–Chem, Atmos. Chem. Phys., 7, 2413–2433, doi:10.5194/acp–7–2413–2007, 2007.

Hoesly R. M., Smith S. J., Feng L. Y., Klimont Z., Janssens-Maenhout G., Pitkanen T., Seibert J. J., Vu L., Andres R. J., Bolt R. M., Bond T. C., Dawidowski L., Kholod N., Kurokawa J., Li M., Liu L., Lu Z. F., Moura M. C. P., O'Rourke P. R., Zhang Q.: Historical (1750–2014) anthropogenic emissions of reactive gases and aerosols from the Community Emissions Data System (CEDS), Geosci. Model Dev., 11, 369–408, 10.5194/gmd-11-369-2018, 2018.

Hogrefe, C., Liu, P., Pouliot, G., Mathur, R., Roselle, S., Flemming, J., Lin, M., and Park, R. J.: Impacts of different characterizations of large-scale background on simulated regional-scale ozone over the continental United States, Atmos. Chem. Phys., 18, 3839–3864, 2018.

Huang, K., Fu, J. S., Hodson, E. L., Dong, X., Cresko, J., Prikhodko, V. Y., Storey, J. M., and Cheng, M.-D.: Identification of missing anthropogenic emission sources in Russia: Implication for modeling Arctic haze, Aerosol Air Qual. Res., 14, 1799–1811, 2014.

Huang, K., Fu, J. S., Prikhodko, V. Y., Storey, J. M., Ro- manov, A., Hodson, E. L., Cresko, J., Morozova, I., Ig- natieva, Y., and Cabaniss, J.: Russian anthropogenic black carbon: Emission reconstruction and Arctic black carbon simulation, J. Geophys. Res.-Atmos., 120, 11306–11333, https://doi.org/10.1002/2015JD023358, 2015.

IPCC: Climate Change: The Intergovernmental Panel on Climate Change Scientific Assessment. The Intergovernmental Panel on Climate Change (IPCC), Cambridge University Press, Cambridge, UK, 1990.

IPCC: Climate Change 2001: The Scientific Basis. Intergovernmental Panel on Climate Change. The Intergovernmental Panel on Climate Change (IPCC), Cambridge University Press, Cambridge, UK, 2001.

Janssens-Maenhout, G., Crippa, M., Guizzardi, D., Dentener, F., Muntean, M., Pouliot, G., Keating, T., Zhang, Q., Kurokawa, J., Wankmüller, R., Denier van der Gon, H., Kuenen, J. J. P., Klimont, Z., Frost, G., Darras, S., Koffi, B., and Li, M.: HTAP_v2.2: a mosaic of regional and global emission grid maps for 2008 and 2010 to study hemispheric transport of air pollution, Atmos. Chem. Phys., 15, 11411-11432, 10.5194/acp-15-11411-2015, 2015.

Jonson, J. E., Schulz, M., Emmons, L., Flemming, J., Henze, D., Sudo, K., Tronstad Lund, M., Lin, M., Benedictow,

A., Koffi, B., Dentener, F., Keating, T., Kivi, R., and Davila, Y.: The effects of intercontinental emission sources on European air pollution levels, Atmos. Chem. Phys., 18, 13655–13672, 2018.

Koch, D. and Hansen, J.: Distant origins of Arctic black carbon: A Goddard Institute for Space Studies ModelE experiment, J. Geophys. Res.–Atmos., 110, D04204, https://doi.org/10.1029/2004JD005296, 2005.

Lamarque, J. F., Emmons, L. K., Hess, P. G., Kinnison, D. E., Tilmes, S., Vitt, F., Heald, C. L., Holland, E. A., Lauritzen, P. H., Neu, J., Orlando, J. J., Rasch, P. J., and Tyndall, G. K.: CAM-chem: description and evaluation of interactive atmospheric chemistry in the Community Earth System Model, Geosci. Model Dev., 5, 369-411, 10.5194/gmd-5-369-2012, 2012.

Law, K. S. and Stohl, A.: Arctic air pollution: origins and impacts, Science, 315, 1537–1540, https://doi.org/10.1126/science.1137695, 2007.

Liang, C.-K., West, J. J., Silva, R. A., Bian, H., Chin, M., Davila, Y., Dentener, F. J., Emmons, L., Flemming, J., Folberth, G., Henze, D., Im, U., Jonson, J. E., Keating, T. J., Kucsera, T., Lenzen, A., Lin, M., Lund, M. T., Pan, X., Park, R. J., Pierce, R. B., Sekiya, T., Sudo, K., and Takemura, T.: HTAP2 multi-model estimates of premature human mortality due to intercontinental transport of air pollution and emission sectors, Atmos. Chem. Phys., 18, 10497–10520, 2018.

Lund, M. T., Berntsen, T. K., Heyes, C., Klimont, Z., and Samset, B. H.: Global and regional climate impacts of black carbon and co-emitted species from the on-road diesel sector, Atmos. Envi- ron., 98, 50–58, https://doi.org/10.1016/j.atmosenv.2014.08.033, 2014.

Lund, M. T., Aamaas, B., Berntsen, T., Bock, L., Burkhardt, U., Fuglestvedt, J. S., and Shine, K. P.: Emission metrics for quantifying regional climate impacts of aviation, Earth Syst. Dynam., 8, 547–563, https://doi.org/10.5194/esd-8-547-2017, 2017.

Lund, M. T., Myhre, G., Haslerud, A. S., Skeie, R. B., Griesfeller, J., Platt, S. M., Kumar, R., Myhre, C. L., and Schulz, M.: Concentrations and radiative forcing of anthropogenic aerosols from 1750 to 2014 simulated with the Oslo CTM3 and CEDS emission inventory, Geosci. Model Dev., 11, 4909–4931, https://doi.org/10.5194/gmd-11-4909-2018, 2018.

Marelle, L., Thomas, J. L., Raut, J.-C., Law, K. S., Jalkanen, J.- P., Johansson, L., Roiger, A., Schlager, H., Kim, J., Reiter, A., and Weinzierl, B.: Air quality and radiative impacts of Arctic shipping emissions in the summertime in northern Norway: from the local to the regional scale, Atmos. Chem. Phys., 16, 2359– 2379, https://doi.org/10.5194/acp-16-2359-2016, 2016.

Miao, Y. C., Guo, J. P., Liu, S. H., Liu, H., Zhang, G., Yan, Y., He, J.: Relay transport of aerosols to Beijing–Tianjin–Hebei region by multiscale atmospheric circulations, Atmos. Environ., 165, 35–45, https://doi.org/10.1016/j.atmosenv.2017.06.032, 2017.

Myhre, G., Shindell, D., Breon, F.–M., Collins, W., Fuglestvedt, J., Huang, J., Koch, D., Lamarque, J.–F., Lee, D., Mendoza, B., Nakajima, T., Robock, A., Stephens, G., Takemura, T., and Zhang, H.: Anthropogenic and Natural Radiative Forcing, in: Climate Change 2013: The Physical Science Basis. Contribution of Working Group I to the Fifth Assessment Report of the Inter– governmental Panel on Climate Change, edited by: Stocker, T. F., Qin, D., Plattner, G.–K., Tignor, M., Allen, S. K., Boschung, J., Nauels, A., Xia, Y., Bex, V., and Midgley, P. M., Cambridge Uni– versity Press, Cambridge, UK and New York, NY, USA, 2013.

Olivié, D. J. L. and Peters, G. P.: Variation in emission metrics due to variation in CO2 and temperature impulse response functions, Earth Syst. Dynam., 4, 267–286, https://doi.org/10.5194/esd-4- 267-2013, 2013.

Paliwal, U., Sharma, M., and Burkhart, J. F.: Monthly and spatially resolved black carbon emission inventory of India: uncertainty analysis, Atmos. Chem. Phys., 16, 12457-12476, 10.5194/acp-16-12457-2016, 2016.

Sahu, S. K., Beig, G., and Sharma, C.: Decadal growth of black carbon emissions in India, Geophysical Research Letters, 35, 10.1029/2007gl032333, 2008.

Samset, B. H., Myhre, G., Schulz, M., Balkanski, Y., Bauer, S., Berntsen, T. K., Bian, H., Bellouin, N., Diehl, T.,

Easter, R. C., Ghan, S. J., Iversen, T., Kinne, S., Kirkevåg, A., Lamarque, J. F., Lin, G., Liu, X., Penner, J. E., Seland, Ø., Skeie, R. B., Stier, P., Takemura, T., Tsigaridis, K., and Zhang, K.: Black carbon vertical profiles strongly affect its radiative forcing uncertainty, Atmos. Chem. Phys., 13, 2423-2434, 10.5194/acp-13-2423-2013, 2013.

Sand, M., Berntsen, T. K., von Salzen, K., Flanner, M. G., Langner, J., and Victor, D. G.: Response of Arctic temperature to changes in emissions of short–lived climate forcers, Nature Clim. Change, 6, 286–289, 10.1038/nclimate2880, 2016.

Sekiya, T., Miyazaki, K., Ogochi, K., Sudo, K., and Takigawa, M.: Global high-resolution simulations of tropospheric nitrogen dioxide using CHASER V4.0, Geosci. Model Dev., 11, 959-988, 10.5194/gmd-11-959-2018, 2018.

Sharma, S., Ishizawa, M., Chan, D., Lavoué, D., Andrews, E., Eleftheriadis, K., and Maksyutov, S.: 16-year simulation of Arctic black carbon: Transport, source contribution, and sensitivity analysis on deposition, Journal of Geophysical Research: Atmospheres, 118, 943-964, 10.1029/2012jd017774, 2013.

Sharma, G., Sinha, B., Pallavi, Hakkim, H., Chandra, B. P., Kumar, A., and Sinha, V.: Gridded Emissions of CO, NO x, SO_2, CO_2, NH_3, HCl, CH_4, $PM_{2.5}$, PM_{10}, BC, and NMVOC from Open Municipal Waste Burning in India, Environ Sci Technol, 53, 4765-4774, 10.1021/acs.est.8b07076, 2019.

Shine, K. P., Fuglestvedt, J. S., Hailemariam, K., and Stuber, N.: Alternatives to the Global Warming Potential for Comparing Climate Impacts of Emissions of Greenhouse Gases, Climatic Change, 68, 281–302, 10.1007/s10584–005–1146–9, 2005

Shindell, D. and Faluvegi, G.: Climate response to regional radiative forcing during the 20th century, Nat. Geosci., 2, 294–300, 2009.

Shindell, D. and Faluvegi, G.: The net climate impact of coal–fired power plant emissions, Atmos. Chem. Phys., 10, 3247–3260, https://doi.org/10.5194/acp–10–3247–2010, 2010.

Shindell D., Kuylenstierna J.C.I., Vignati E., van Dingenen R., Amann M., Klimont Z., Anenberg S.C., Muller N., JanssensMaenhaut G., Raes F., Schwartz J., Faluvegi G., Pozzoli L., Kupiainen K., Höglund–Isaksson L., Emberson L., Streets D., Ramanathan V., Hicks K., Kim Oanh N.T., Milly G., Williams M., Demkine W., Fowler D.: Simultaneously Mitigating Near–Term Climate Change and Improving Human Health and Food Security. Science, Vol. 335, 183–189, 2012.

Shindell, D. T., Chin, M., Dentener, F., Doherty, R. M., Faluvegi, G., Fiore, A. M., Hess, P., Koch, D. M., MacKenzie, I. A., Sanderson, M. G., Schultz, M. G., Schulz, M., Stevenson, D. S., Teich, H., Textor, C., Wild, O., Bergmann, D. J., Bey, I., Bian, H., Cuvelier, C., Duncan, B. N., Folberth, G., Horowitz, L. W., Jonson, J., Kaminski, J. W., Marmer, E., Park, R., Pringle, K. J., Schroeder, S., Szopa, S., Takemura, T., Zeng, G., Keating, T. J., Zuber, A.: A multi–model assessment of pollution transport to the Arctic, Atmos. Chem. Phys. Discuss., 2008.

Shindell, D. T., Faluvegi, G., Rotstayn, L., and Milly, G.: Spatial patterns of radiative forcing and surface temperature response, J. Geophys. Res.-Atmos., 120, 5385–5403, https://doi.org/10.1002/2014JD022752, 2015.

Shindell, D. T., Lamarque, J.–F., Schulz, M., Flanner, M., Jiao, C., Chin, M., Young, P. J., Lee, Y. H., Rotstayn, L., Mahowald, N., Milly, G., Faluvegi, G., Balkanski, Y., Collins, W. J., Conley, A. J., Dalsoren, S., Easter, R., Ghan, S., Horowitz, L., Liu, X., Myhre, G., Nagashima, T., Naik, V., Rumbold, S. T., Skeie, R., Sudo, K., Szopa, S., Takemura, T., Voulgarakis, A., Yoon, J.–H., and Lo, F.: Radiative forcing in the ACCMIP historical and future climate simulations, Atmos. Chem. Phys., 13, 2939–2974, 2013.

Shindell, D. T., Voulgarakis, A., Faluvegi, G., and Milly, G.: Precipitation response to regional radiative forcing, Atmos. Chem. Phys., 12, 6969–6982, doi:10.5194/acp–12–6969–2012, 2012.

Smith, S.J. and Mizrahi, A.: Near–term climate mitigation by short–lived forcers. PNAS 14202–14206, doi:

10.1073/pnas.1308470110, 2013.

Sobhani, N., Kulkarni, S., Carmichael, G. R.: Source sector and region contributions to black carbon and $PM_{2.5}$ in the Arctic. Atmos. Chem. Phys., 18, 18123–18148, 2018.

Stjern, C. W., Samset, B. H., Myhre, G., Bian, H., Chin, M., Davila, Y., Dentener, F., Emmons, L., Flemming, J., Haslerud, A. S., Henze, D., Jonson, J. E., Kucsera, T., Lund, M. T., Schulz, M., Sudo, K., Takemura, T., and Tilmes, S.: Global and regional radiative forcing from 20 % reductions in BC, OC and SO4 – an HTAP2 multi-model study, Atmos. Chem. Phys., 16, 13579–13599, https://doi.org/10.5194/acp-16-13579-13599, 2016.

Stjern, C. W. et al. Rapid adjustments cause weak surface temperature response to increased black carbon concentrations. Geophys. Res. 122, 11462–11481, 2017.

Stohl, A.: Characteristics of atmospheric transport into the Arctic troposphere, J. Geophys. Res., 111, D11306, https://doi.org/10.1029/2005JD006888, 2006.

Stohl A., Aamaas B., Amann M., Baker L. H., Bellouin N., Berntsen T. K., Boucher O., Cherian R., Collins W., Daskalakis N., Dusinska M., Eckhardt S., Fuglestvedt J. S., Harju M., Heyes C., Hodnebrog Ø., Hao J., Im U., Kanakidou M., Klimont Z., Kupiainen K., Law K. S., Lund M. T., Maas R., MacIntosh C. R., Myhre G., Myriokefalitakis S., Olivié D., Quaas J., Quennehen B., Raut J.–C., Rumbold S. T., Samset B. H., Schulz M., Seland Ø., Shine K. P., Skeie R. B., Wang S., Yttri K. E., and Zhu T.: Evaluating the climate and air quality impacts of short–lived pollutants. Atmos. Chem. Phys., 15, 10529 – 10566, 2015.

Stohl, A., Eckhardt, S., Forster, C., James, P., and Spichtinger, N.: On the pathways and timescales of intercontinental air pollution transport, J. Geophys. Res.–Atmos., 107, ACH 6–1–ACH 6–17, https://doi.org/10.1029/2001JD001396, 2002.

Stohl, A., Klimont, Z., Eckhardt, S., Kupiainen, K., Shevchenko, V. P., Kopeikin, V. M., and Novigatsky, A. N.: Black carbon in the Arctic: the underestimated role of gas flaring and residential combustion emissions, Atmos. Chem. Phys., 13, 8833–8855, https://doi.org/ 10.5194/acp-13-8833-2013, 2013

Sudo, K., Sekiya, T., Nagashima, T.: CHASER/MIROC-ESM in HTAP2 status reports, HTAP2 Global and Regional Model Evaluation Workshop, Nagoya University, JAMSTEC, NIES, 2015.

Sudo, K., Takahashi, M., Kurokawa, J.–I., and Akimoto, H.: CHASER: A global chemical model of the troposphere 1. Model description, J. Geophys. Res.–Atmos., 107, ACH 7–1–ACH 7–20, doi:10.1029/2001JD001113, 2002.

Søvde, O. A., Prather, M. J., Isaksen, I. S. A., Berntsen, T. K., Stordal, F., Zhu, X., Holmes, C. D., and Hsu, J.: The chemical transport model Oslo CTM3, Geosci. Model Dev., 5, 1441–1469, doi:10.5194/gmd–5–1441–2012, 2012.

Takemura, T., and Suzuki, K.: Weak global warming mitigation by reducing black carbon emissions, Scientific Reports, 9, 10.1038/s41598-019-41181-6, 2019.

Tan, J., Fu, J. S., Dentener, F., Sun, J., Emmons, L., Tilmes, S., Sudo, K., Flemming, J., Jonson, J. E., Gravel, S., Bian, H., Davila, Y., Henze, D. K., Lund, M. T., Kucsera, T., Takemura, T., and Keating, T.: Multi-model study of HTAP II on sulfur and nitrogen deposition, Atmos. Chem. Phys., 18, 6847–6866, 2018a.

Tan, J., Fu, J. S., Dentener, F., Sun, J., Emmons, L., Tilmes, S., Flemming, J., Takemura, T., Bian, H., Zhu, Q., Yang, C.-E., and Keating, T.: Source contributions to sulfur and nitrogen deposition – an HTAP II multi-model study on hemispheric transport, Atmos. Chem. Phys., 18, 12223–12240, 2018b.

Teng, H., Washington, W. M., Branstator, G., Meehl, G. A., and Lamarque, J.–F.: Potential impacts of Asian carbon aerosols on future US warming, Geophys. Res. Lett., 39, L11703, doi:10.1029/2012GL051723, 2012.

Tilmes, S., Lamarque, J.–F., Emmons, L. K., Kinnison, D. E., Marsh, D., Garcia, R. R., Smith, A. K., Neely, R. R., Conley, A., Vitt, F., Val Martin, M., Tanimoto, H., Simpson, I., Blake, D. R., and Blake, N.: Representation of the Community Earth System Model (CESM1) CAM4–chem within the Chemistry– Climate Model Initiative

(CCMI), Geosci. Model Dev., 9, 1853– 1890, doi:10.5194/gmd–9–1853–2016, 2016.

Twomey, S.: The influence of pollution on the shortwave albedo of clouds, J. Atmos. Sci., 34, 1149–1152, 1977.

UNEP/WMO: Integrated Assessment of Black Carbon and Tropospheric Ozone, Nairobi, Kenya, available at: http://wedocs.unep.org/handle/20.500.11822/8028 (last access: 13 May 2020), 2011.

US EPA: Guidance on the use of models and other analyses for demonstrating attainment of air quality goals for ozone, $PM_{2.5}$, and regional haze. U.S. Environmental Protection Agency Office of Air Quality Planning and Standards Air Quality Analysis Division Air Quality Modeling Group Research Triangle Park, NC, 2007.

Zhang, H. Y., Cheng, S. Y., Yao, S., Wang, X. Q., and Zhang, J. F.: Multiple perspectives for modeling regional $PM_{2.5}$ transport across cities in the Beijing–Tianjin–Hebei region during haze episodes, Atmos. Environ., 212, 22–35, https://doi.org/10.1016/j.atmosenv.2019.05.031, 2019.

Zhang, X., Zhang, Y. H, Han, J. B., Zhang, L., and Shi, W. R.: Analysis of the climatic characteristics of the atmospheric boundary layer height in yanmayan Island, Arctic (in Chinese), Polar studies, 30(02):132–139, 2018.